Existence and stability analysis of finite 0-π-0 Josephson junctions

Saeed Ahmad,* Hadi Susanto, and Jonathan A. D. Wattis
School of Mathematical Sciences, University of Nottingham, University Park, Nottingham NG7 2RD, United Kingdom
(Received 9 March 2009; revised manuscript received 1 July 2009; published 27 August 2009)

We investigate analytically and numerically a Josephson junction on a finite domain with two π-discontinuity points characterized by a jump of π in the phase difference of the junction, that is, a 0-π-0 Josephson junction. The system is described by a modified sine-Gordon equation. We show that there is an instability region in which semifluxons are spontaneously generated. Using a Hamiltonian energy characterization, it is shown that the existence of static semifluxons depends on the length of the junction, the facet length, and the applied bias current. The critical eigenvalue of the semifluxons is discussed as well. Numerical simulations are presented, supporting our analytical results.

DOI: 10.1103/PhysRevB.80.064515 PACS number(s): 74.50.+r

I. INTRODUCTION

Josephson junctions are made of two superconductors connected by a nonsuperconducting weak link. Interestingly, a current can flow from one superconductor to the other even when there is no potential difference, i.e., the Josephson supercurrent. Current technological advances can impose artificial shifts to the Josephson phase, such that the sign of the critical current depends on the spatial variable.

The idea of having a shift in the gauge phase of a Josephson junction was first proposed by Bulaevskii *et al.*[1,2] It was proposed that the presence of the magnetic impurities may create a π shift to the Josephson phase, which has been confirmed recently.[3] Presently, one can also impose a π phase shift in a long Josephson junction using superconductors with unconventional pairing symmetry,[4,5] superconductor-ferromagnet-superconductor (SFS) π junctions,[6] superconductor-insulator-ferromagnet-superconductor (SIFS) π and 0-π junctions,[7,8] superconductor-normal metal-superconductor (SNS) junctions,[9] or using a pair of current injectors.[10] All these findings have promising applications in information storage and information processing.[11,12] This system, in which neighboring facets of a Josephson junction are considered to have opposite signs of the critical current, present intriguing phenomena such as the intrinsic frustration of the Josephson phase over the junction and the spontaneous generation of a fractional magnetic flux at the discontinuities, that is, the positions of the jumps in the Josephson phase.[13,14]

In the present work, we consider the so-called 0-π-0 Josephson junctions on a finite domain, modeled by a modified sine-Gordon equation with phase shift of $\theta=\pi$ in some region and zero otherwise. An infinite domain 0-π-0 Josephson junction was first studied by Kato and Imada,[15] where they showed that there is a stability window for the π junction length in which the uniform zero solution is stable. In the instability region, the ground state is a nonuniform solution, which corresponds to a pair of antiferromagnetically ordered semifluxons. Later, it was shown that there is a minimum facet length of the π junction, above which a nontrivial ground state exits, which corresponds to the minimum facet length needed to construct such solutions,[16,17] that is the bifurcation is supercritical. The possibility of employing a 0-π-0 junction for observing macroscopic quantum tunneling was discussed in length by Goldobin *et al.*[18] In the presence of an applied bias current, a 0-π-0 Josephson junction has a critical current above, which one can flip the order of the semifluxons[15,19,20] and another critical current above which the junction switches to the resistive state.[17,21] Goldobin *et al.*[22,23] have also broadened the study of 0-π-0 junctions to 0-κ-0 junctions, where $0\leq\kappa\leq\pi$ (mod 2π). Here, we limit ourselves to discuss 0-π-0 junctions only, but extend it to the case of a finite domain. This is of particular interest, especially from the physical point of view, since such junctions have recently been successfully fabricated,[19,20] making a finite length analysis more relevant.

The present paper is structured as follows. In Sec. II, we discuss the mathematical model that we use to describe the problem. We then show in Sec. III that when there is no bias current, the equation has two uniform solutions. Due to the phase shifts, there will be a region of facet lengths, in which both uniform solutions are unstable. In this instability region, a nonuniform ground state will emerge from the uniform solutions, i.e., a pair of semifluxons is the ground state of the system. A Hamitonian analysis is performed in Sec. IV to study the behavior of the non-trivial ground state, both with and without the presence of an applied bias current. We compare our analytical results with numerical computations in Sec. V. Finally, conclusions are presented in Sec. VI.

II. MATHEMATICAL MODEL

The dynamics of a finite Josephson junction with π-discontinuity points is commonly described by the following perturbed sine-Gordon equation

$$\phi_{xx}-\phi_{tt}=\sin[\phi+\theta(x)]-\gamma+\alpha\phi_t, \quad -L\leq x\leq L, \quad (1)$$

where α is a dimensionless positive damping coefficient related to quasi-particle tunneling across the junction, $2L$ is the total length of the junction, and γ is the applied bias current density normalized to the junction critical current density J_c. Equation (1) is written after rescaling where the spatial variable x and time variable t are normalized to the Josephson penetration length λ_J and the inverse plasma frequency ω_p^{-1}, respectively.

The function θ, representing the presence, or absence, of the additional π-phase shift, is given by

$$\theta(x) = \begin{cases} 0, & L > |x| > a, \\ \pi, & |x| < a, \end{cases} \tag{2}$$

where $2a$ is the length of the π-junction, which we refer to as the facet length. This is our primary bifurcation parameter in the ensuing analysis.

Equation (1) is subject to the continuity and boundary conditions

$$\phi(\pm a^-) = \phi(\pm a^+), \quad \phi_x(\pm a^-) = \phi_x(\pm a^+), \quad \phi_x(\pm L) = 0. \tag{3}$$

The governing Eq. (1) with $\alpha=0$, subject to the boundary conditions (3), can be derived from the Lagrangian

$$\mathcal{L} = \int_{-L}^{L} \left[\frac{1}{2}\phi_t^2 - \frac{1}{2}\phi_x^2 - 1 + \cos(\phi + \theta) - \gamma\phi \right] dx. \tag{4}$$

As we mainly consider static semifluxons, the existence of the solutions will be studied through the time-independent version of (1), namely

$$\phi_{xx} = \sin(\phi + \theta) - \gamma. \tag{5}$$

III. EXISTENCE AND STABILITY ANALYSIS OF UNIFORM SOLUTIONS

It is clear that Eq. (5) admits two uniform solutions (modulo 2π), namely

$$\tilde{\phi} = \arcsin\ \gamma, \quad \pi - \arcsin\ \gamma,$$

for $a<|x|<L$, and

$$\tilde{\phi} = \arcsin\ \gamma - \pi, \quad -\arcsin\ \gamma,$$

for $0<|x|<a$.

As solutions on the whole domain must satisfy the continuity conditions (3), we conclude that uniform solutions exist only when $\gamma=0$, hence $\tilde{\phi}=0$ and $\tilde{\phi}=\pi$.

Next, we determine the linear stability of the uniform solutions. For this purpose, we substitute the stability ansatz

$$\phi = \tilde{\phi} + \epsilon e^{\lambda t} V(x) \tag{6}$$

into Eq. (1). Neglecting higher order terms in ϵ, one obtains the eigenvalue problem

$$V_{xx} = [E + \cos(\tilde{\phi} + \theta)]V, \tag{7}$$

where

$$E = \lambda^2 + \alpha\lambda \tag{8}$$

and V is also subject to the continuity and boundary conditions

$$V(\pm a^-) = V(\pm a^+), \quad V_x(\pm a^-) = V_x(\pm a^+), \quad V_x(\pm L) = 0. \tag{9}$$

Because the eigenvalue problem (7) is self-adjoint, the spectral parameter E (8) will be real valued. One will obtain that

$$\lambda_{\pm} = \frac{1}{2}(-\alpha \pm \sqrt{\alpha^2 + 4E}).$$

When $E>0$, it can be concluded that $\mathrm{Re}(\lambda_-)<0$ and $\mathrm{Re}(\lambda_+)>0$. One can also easily calculate that when $E\leq 0$, $\mathrm{Re}(\lambda_\pm)\leq 0$. From the stability ansatz (6), it is clear that $\tilde{\phi}$ is stable if λ has nonpositive real parts. Therefore, a solution $\tilde{\phi}$ is said to be linearly stable if $E<0$ and unstable when $E>0$. Because the stability of a solution is rather determined by the sign of E, this informs us that an unstable solution at $\alpha=0$ will remain unstable in the dissipative system $\alpha\neq 0$. Therefore, without loss of generality, in the following we set $\alpha=0$.

Due to the finite size of the domain, the eigenvalue problem (7) will give two sets of eigenvalues, an infinite set that constitutes the continuous spectrum and a finite set in the discrete spectrum. For simplicity, in the following sections we refer to the infinite set the "continuous" spectrum.

A. Linear stability of the uniform 0 solution

First, we discuss the "continuous" spectrum of $\tilde{\phi}=0$.

Looking for a bounded solution to (7) that satisfies the boundary conditions at $x=\pm L$, we obtain the solutions

$$V(x) = \begin{cases} A\cos[\hat{\alpha}(x+L)], & -L < x < -a, \\ B\cos(\hat{\beta}x) + C\sin(\hat{\beta}x), & |x| < a, \\ D\cos[\hat{\alpha}(x-L)], & a < x < L, \end{cases} \tag{10}$$

where $\hat{\alpha}=\sqrt{-1-E}$ and $\hat{\beta}=\sqrt{1-E}$.

Using the continuity conditions (9), we obtain a system of four equations with four unknowns, given in a matrix form by

$$M_1 \begin{pmatrix} A \\ B \\ C \\ D \end{pmatrix} = 0,$$

with a coefficient matrix M_1 given in the Appendix.

To obtain a nontrivial V, we require $\det(M_1)=0$. An implicit plot of this equation, that is, the "continuous" spectrum $E(a,L)$, for $L=1$ is shown in the top panel of Fig. 1. Numerically, it is found that there is no unstable eigenvalue in the 'continuous' spectrum, i.e., $E<0$ for all a. As L increases, the distribution of E will become dense, as expected.

Next, we find the discrete spectrum of the uniform solution $\tilde{\phi}=0$, corresponding to bounded and decaying solutions of the eigenvalue problem (7). We obtain the solution

$$V(x) = \begin{cases} A\cosh[\hat{\gamma}(x+L)], & -L < x < -a, \\ B\cos(\hat{\beta}x) + C\sin(\hat{\beta}x), & |x| < a, \\ D\cosh[\hat{\gamma}(x-L)], & a < x < L, \end{cases} \tag{11}$$

where $\hat{\gamma}=\sqrt{1+E}$ and $\hat{\beta}$ is defined above.

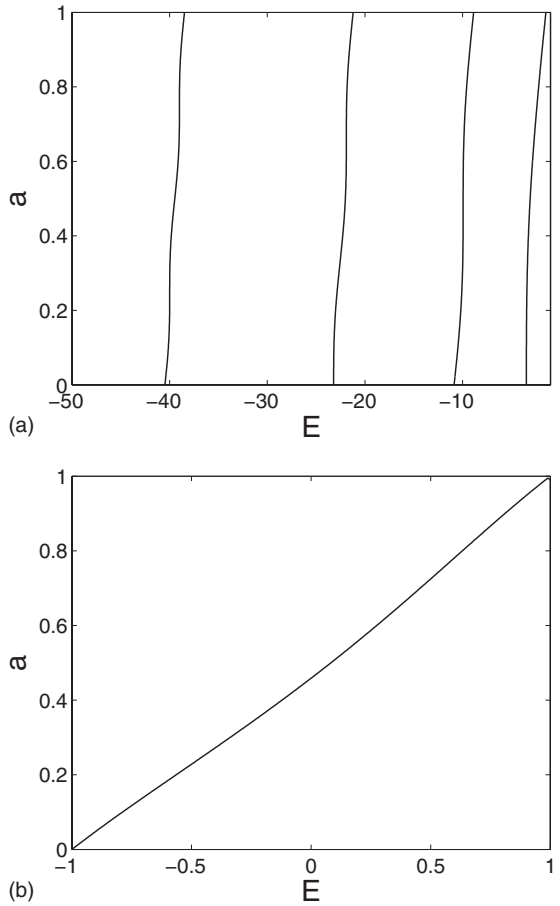

FIG. 1. Plot of the "continuous" spectrum (top) and the discrete spectrum (bottom) of $\tilde{\phi}=0$ as a function of half of the π junction length a for $L=1$.

From the continuity conditions, again we find a system of four equations. As above, the eigenvalues are obtained by setting the determinant of the coefficient matrix M_2, given in the Appendix, to zero. An implicit plot of the eigenvalues as a function of a for $L=1$ is shown in the bottom panel of Fig. 1.

From Fig. 1, we observe that for a given L, there is a critical a above which E becomes positive, i.e., $\tilde{\phi}=0$ becomes unstable. In the following, we denote such a critical a by $a_{c,0}$. For $L=1$, $a_{c,0}\approx 0.46$. As L increases, $a_{c,0}$ will asymptotically approach $\frac{\pi}{4}$, which is the critical length in the infinite domain calculated in Refs. 15 and 17. The relation between $a_{c,0}$ and L is implicitly given by the smallest positive root of

$$\cot(a_{c,0})\tanh(L-a_{c,0})=1, \tag{12}$$

which is obtained by considering the even mode of (11), for which $E=C=0$ and $A=D=B\cos(a_{c,0})/\cosh(L-a_{c,0})$. For small L the root can be approximated by

$$a_{c,0}=\frac{L}{2}-\frac{1}{24}L^3+\mathcal{O}(L^5). \tag{13}$$

Plots of $a_{c,0}$ as a function of L given implicitly by (12) and its approximation (13) are shown in Fig. 3.

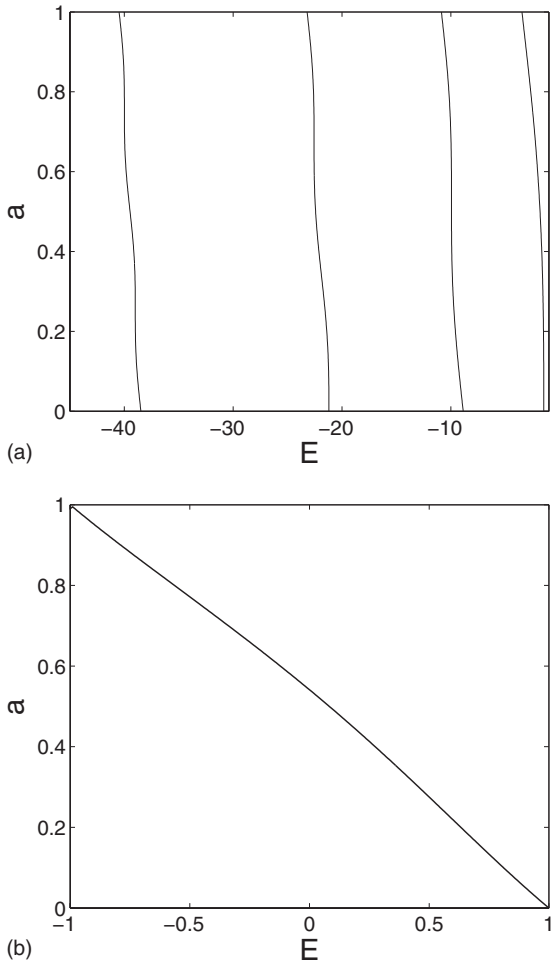

FIG. 2. The same as Fig. 1, but for $\tilde{\phi}=\pi$.

B. Linear stability of the uniform π solution

Following the same steps as we did in the stability analysis of $\tilde{\phi}=0$, the solution V to the eigenvalue problem (7) that corresponds to the 'continuous' spectrum is given by

$$V(x)=\begin{cases} A\cos[\hat{\beta}(x+L)], & -L<x<-a, \\ B\cos(\hat{\alpha}x)+C\sin(\hat{\alpha}x), & |x|<a, \\ D\cos[\hat{\beta}(x-L)], & a<x<L. \end{cases} \tag{14}$$

One then finds that the spectrum is given by the zero of the determinant of the coefficient matrix M_3, given in the Appendix.

A plot of the "continuous" spectrum in the (E,a) plane is shown in Fig. 2, from which it is clear that the continuous spectrum also only consists of stable eigenvalues.

For the discrete spectrum of $\tilde{\phi}=\pi$ in a finite domain, bounded and decaying solutions V of the eigenvalue problem (7) are given by

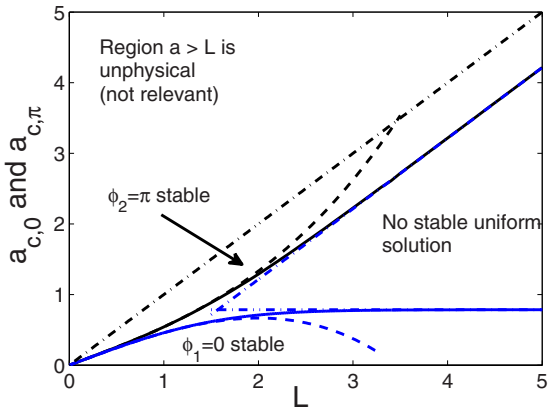

FIG. 3. (Color online) Instability region of the uniform solutions $\tilde{\phi}=0$ and $\tilde{\phi}=\pi$. Solid boundary curves are given by Eqs. (12) and (16). Dashed lines are analytical approximations for small L given by (13) and (17). Dashed dotted lines are analytical approximations for large L, $a_{c,0}=\pi/4$, and $a_{c,\pi}=L-\pi/4$.

$$V(x)=\begin{cases} A\cos[\hat{\beta}(x+L)], & (-L<x<-a), \\ B\cosh(\hat{\gamma}x)+C\sinh(\hat{\gamma}x), & (|x|<a), \\ D\cos[\hat{\beta}(x-L)], & (a<x<L). \end{cases} \tag{15}$$

Due to the boundary conditions (9), again we obtain a system of four homogenous equations with a coefficient matrix M_4, given in the Appendix.

The bottom panel of Fig. 2 shows the plot of the zeros of $\det(M_4)$ in the (E,a) plane, for $L=1$. We observe that for a close to zero, $E>0$, i.e., $\tilde{\phi}=\pi$ is unstable. Yet, there is a critical value of a above which $\tilde{\phi}=\pi$ is stable. We denote this critical length by $a_{c,\pi}$, which for $L=1$ is approximately 0.54.

Again, considering the even state of (15), we have $E=C=0$ and $A=D=B\cosh(a_{c,\pi})/\cos(L-a_{c,\pi})$, one can show that $a_{c,\pi}$ is related to L by the implicit equation

$$\coth(a_{c,\pi})\tan(L-a_{c,\pi})=1, \tag{16}$$

which, for small L, can be approximated by

$$a_{c,\pi}=\frac{L}{2}+\frac{1}{24}L^3+\mathcal{O}(L^5). \tag{17}$$

Combining Eqs. (12) and (16), we plot in Fig. 3 the region in which *both* the stationary solutions of the sine-Gordon (1) are unstable. In the instability region, the ground state will be nonuniform.

C. Symmetry

Comparing Figs. 1 and 2, we observe that they are the same by reflection with respect to the line $a=L/2=1/2$, that is, the stability of $\phi=0$ at the half facet length a is the same as the stability of $\phi=\pi$ at the half facet length $(L-a)$. This symmetry occurs because, for the particular solutions, our Neumann boundary conditions at $x=\pm L$ (3) can be replaced by periodic boundary conditions

$$\phi(-L)=\phi(L), \quad \phi_x(-L)=\phi_x(L). \tag{18}$$

For the periodic boundary conditions, the governing Eq. (1) is symmetric by rotation, i.e., cyclic symmetry, and $\theta\to\theta+\pi$. Using the symmetry, one can also conclude that

$$a_{c,\pi}=L-a_{c,0}, \tag{19}$$

for any L.

Due to the similarity to a periodic system, our problem in the undriven case $\gamma=0$ is the same as that considered in Ref. 24. As a consequence, Eqs. (11) and (12) [and hence Eqs. (15) and (16)] above are the same as Eqs. (3) and (4) of Ref. 24. Despite the similarity, finite and periodic junctions also have some fundamental differences. These include the fact that continuous spectrum is present in periodic junctions with band gap structures possibly formed in their plasma wave frequency (see, e.g., Ref. 25). Moreover, we conjecture that all the "continuous" eigenfrequencies of a finite Josephson junction can be parasitic that may need to be avoided in finite Josephson junction based devices and that they may be measured using microwave spectroscopy.[26–28] This issue will be addressed in a future publication.

IV. GROUND STATES IN THE INSTABILITY REGION

In the following, we analyze perturbatively the ground states of the Josephson junction in the instability region. Our analysis, based on an Euler-Lagrange approximation, is carried out for a half facet length a close to one of the critical lengths $a_{c,0}$, $a_{c,\pi}$.

A. *Case of* $0<a-a_{c,0}\ll 1$

1. Existence analysis

For a close to $a_{c,0}$, we approximate $\phi(x)$ by

$$\phi(x)=B\begin{cases} \dfrac{\cos(a_{c,0})}{\cosh(L-a_{c,0})}\cosh(x+L), & a<|x|<L, \\ \cos(x), & |x|<a, \end{cases} \tag{20}$$

where $B=B(t)$ and $a_{c,0}$ is given by (12). This expression of ϕ is an exact solution of the linearization of (5) for $a=a_{c,0}$ with an arbitrary parameter B, i.e., we approximate the ground states by $\phi=V(x)$, where $V(x)$ is the first even solution of the eigenvalue problem (7) with $E=0$ and $a=a_{c,0}$.

Substituting the ansatz (20) into the Lagrangian (4), writing $a=L/2-kL^3$, $k<1/24$, and expanding about $L=0$ yields

$$\mathcal{L}=(L-L^3/4)B_t^2-H, \tag{21}$$

where the subscript represents a derivative and

$$H=\frac{L^3B^2}{12}\left[24k-1-\frac{B^2}{3}(6k-1)\right] +2L\left[B\gamma+1-L^2\left(\frac{B\gamma}{8}+2k\right)\right], \tag{22}$$

is the potential energy of the system.

The Euler-Lagrange equation is derived from the Lagrangian (21) by $\partial_t(\partial_{B_t}\mathcal{L})-\partial_B\mathcal{L}=0$, giving

$$B_{tt}=\frac{-1}{2L-L^3/2}H_B. \tag{23}$$

The time independent solution $B=B_0^{(2,3)}$ is given by the cubic equation $H_B=0$, or

$$\gamma(B_0)=-\frac{2L^2B_0[B_0^2(12k-2)+3-72k]}{9(L^2-8)}. \tag{24}$$

For a general value of $\gamma\neq 0$, we solve the cubic equation using Nickalls' method[29] to obtain

$$B_0^{(n)}=2\Delta\cos(\Theta+2(n-1)\pi/3),\quad n=1,2,3, \tag{25}$$

where

$$\Delta=\sqrt{\frac{1-24k}{2-12k}},\quad \Theta=\arccos(-y_N/h)/3,$$

$$y_N=(2L-L^3/4)\gamma,\quad h=-\frac{1}{9}L^3(1-24k)\Delta.$$

When $\gamma=0$, the expressions for $B_0^{(n)}$ are simplified to

$$B_0^{(1,2)}=\pm\sqrt{\frac{3(24k-1)}{2(6k-1)}},\quad B_0^{(3)}=0. \tag{26}$$

The nonzero roots $B_0^{(1,2)}$ represent a pair of antiferromagnetically ordered semifluxons.

If we study further, the three roots (25), we find that they do not persist for all γ. If γ is decreased (increased) away from zero, then there is a critical value of the bias current γ at which $B_0^{(1)}(B_0^{(2)})$ collides with $B_0^{(3)}$ in a saddle node bifurcation. Here, we denote this critical value of γ by $\gamma_{c,1}$. From our current approximation, $\gamma_{c,1}$ can be calculated from the condition $y_N^2=h^2$,[29] which gives

$$\gamma_{c,1}=\frac{2\sqrt{2}L^2(24k-1)^{3/2}}{9\sqrt{6k-1}(L^2-8)}. \tag{27}$$

This critical value can also be obtained by solving $\frac{d\gamma}{dB_0}=0$ from (24) to find B_{0c} and substituting the values for $B_0=B_{0c}$ back into (24) to give $\gamma_{c,1}=\gamma(B_{0c})$.

2. Stability analysis

To study the stability of the stationary solutions (25), we easily check that when $k<1/24$, H is locally minimized by $B_0^{(1,2)}$. To obtain the critical eigenvalue of the stable solutions, we write $B=B_0^{(n)}+\epsilon\tilde{B}$ and substitute this into the Euler-Lagrange Eq. (23) to obtain

$$\ddot{\tilde{B}}(t)=\left.\frac{-1}{2L-L^3/2}\partial_B^2H\right|_{B=B_0^{(n)}}\tilde{B}. \tag{28}$$

The critical eigenvalue of $B_0^{(n)}$ is then given by

$$E=\left.\frac{-1}{(2L-L^3/2)}\partial_B^2H\right|_{B=B_0^{(n)}}, \tag{29}$$

that is, the negative square of the oscillation frequency of $\tilde{B}(t)$.

B. *Case of* $0<a_{c,\pi}-a\ll 1$

To discuss the existence and stability of ground state solutions when a is close to $a_{c,\pi}$, we repeat the above calculations. We exploit the symmetry discussed in Sec. III C, that for the nonuniform ground state, the Neumann boundary conditions (3) can be replaced by periodic boundary conditions (18). Using this symmetry, we obtain that if $\phi(x;a)$ is a ground state solution of the sine-Gordon equation with the π facet length $2a$, then

$$\phi(x;L-a)=\pi-\phi(L-|x|;a). \tag{30}$$

Thus, the stability of the ground state in the limit $0<a_{c,\pi}-a\ll 1$ can be deduced from the case $0<a-a_{c,o}\ll 1$ using this symmetry argument since $a_{c,\pi}=L-a_{c,0}$ (19).

V. DISCUSSION

To check our analytical results, we perform numerical calculations and simulations. We numerically solve the time-independent governing Eq. (5), subject to boundary conditions (3) using a Newton-Raphson method, where we discretize the problem using central differences with a relatively fine spatial discretization. To numerically study the stability of a solution, we then discretize and solve the corresponding linear eigenvalue problem [cf. Equation (7)].

First, we study the existence and the stability of the nonzero ground state in the absence of an applied bias current.

In the top panel of Fig. 4, we plot $\phi(0)$ and $\phi(\pm L)$, of the nonuniform ground states as functions of a for $\gamma=0$ and $L=1$. Due to the cyclic symmetry discussed in Sec. III C, we observe that the curves are symmetric under rotation by π radians, with the center of rotation $(a,\phi)=(L/2,\pi/2)$. In the same figure, we also depict our analytic approximation (26), where one can see a rather good agreement for a near to $a_{c,0}$ and $a_{c,\pi}$.

In the bottom panel of the same figure, we depict the critical eigenvalue of the nonzero ground states presented at the top panel. At the critical facet lengths, the eigenvalues are certainly zero due to the change of stability with the uniform solutions $\phi=0,\pi$. Our analytical approximation (29) is plotted in the same figure, from which we see that when the half facet length a is close to one of the critical values $a_{c,0}$ or $a_{c,\pi}$, the numerics are indeed well approximated by our analytical result.

Next, we study the influence of an applied bias current to the existence and stability of the nonuniform ground state. In the following, we particularly consider $a=0.495$ and without loss of generality the "positive" ground state, $\phi(0)>0$. The case of negative $\phi(0)$ can be obtained simply by reflection due to the symmetry $\phi\to-\phi$ and $\gamma\to-\gamma$.

In the top panel of Fig. 5, we plot our numerical $\phi(0)$ as a function of the applied bias current γ for $L=1$ and a

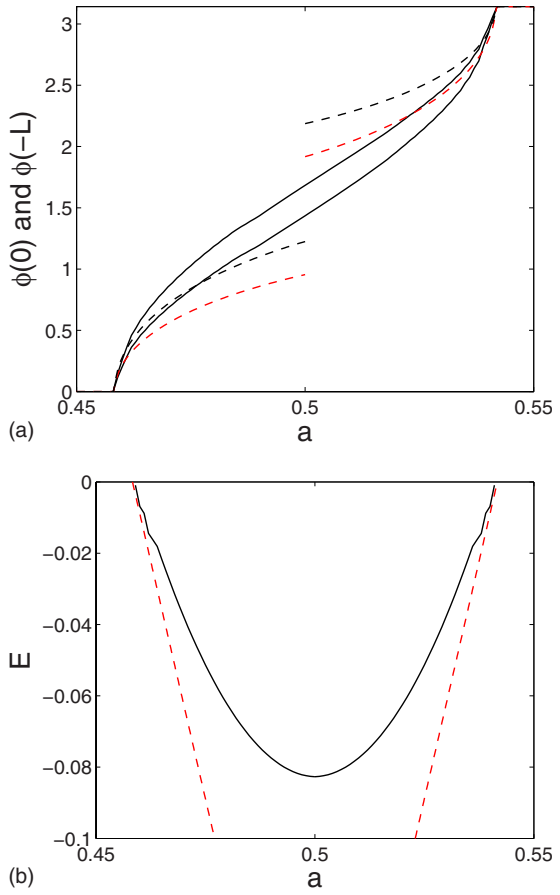

FIG. 4. (Color online) (Top) Plot of $\phi(0)$ and $\phi(\pm L)$ of the nonuniform ground state obtained from numerical calculations (solid lines) as a function of half of the facet length a. Comparison with our analytical approximations (dashed lines) is also presented. (Bottom) The critical eigenvalue E of the solution depicted in the bottom panel.

$=0.495$. We use a path-following method starting from $\gamma=0$ and $\phi(0)\approx 0.16$.

First, we decrease the applied bias current. As γ is reduced, the value of $\phi(0)$ also decreases up to a certain value of bias current; the solution cannot be continued further, it terminates in a saddle node bifurcation. Using our path following method, the saddle-node bifurcation is indeed due to a collision with a nonuniform solution bifurcating from $\tilde{\phi}=0$, as predicted by our analytical result. The value of $\gamma<0$ at which the bifurcation occurs is the aforementioned $\gamma_{c,1}$ (27). Comparisons between the numerics and the analytical results of $\gamma_{c,1}$ are depicted at the middle panel of Fig. 5.

Besides decreasing γ, one can also increase it. As γ increases, the value of $\phi(0)$ also increases. As the bias current is increased further, a saddle-node bifurcation occurs. We denote this critical value of bias current by $\gamma_{c,2}$. Using our path following algorithm, we can follow the upper branch of the bifurcation and deduce that it corresponds to a collision between the nonuniform solution and the solution which bifurcates from $\tilde{\phi}=\pi$. Using the cyclic symmetry argument, we explain the bifurcation using our analytical results (25). Plotted in the top panel of Fig. 5 is our $\gamma(B_0)$ given by Eq. (24), properly shifted by π, for the half facet length $(L-a)$.

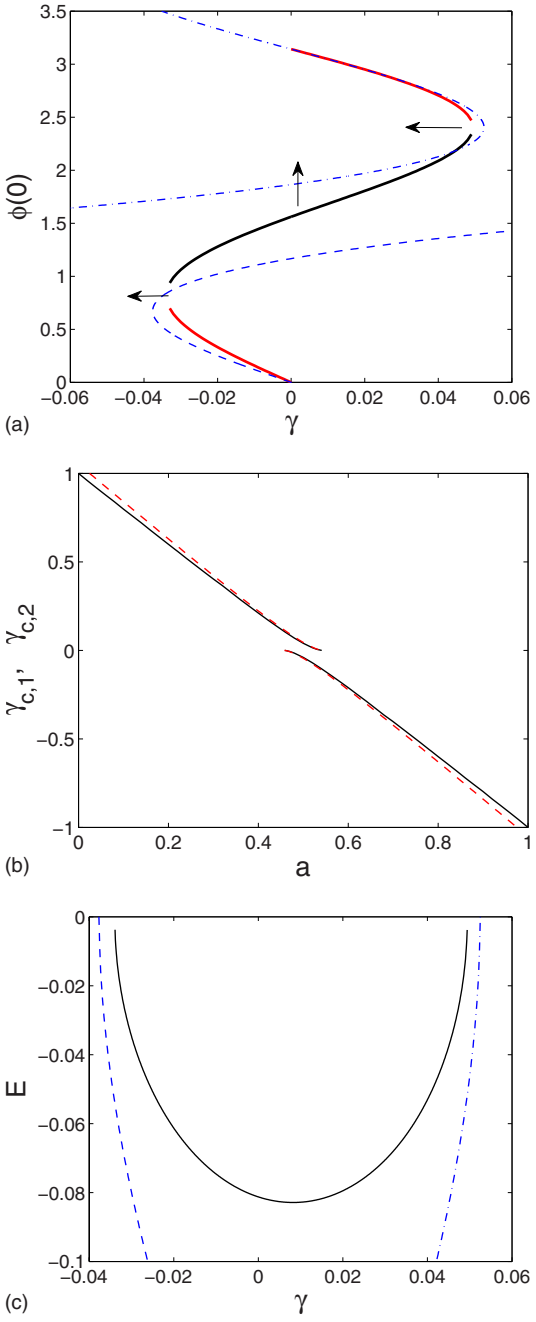

FIG. 5. (Color online) The top panel depicts the existence diagram of the ground state. Plotted is $\phi(0)$ as a function of γ, obtained from numerical computations (solid lines) for $a=0.495$ and $L=1$. Shown in red is $\phi(0)$ as a function of a that corresponds to unstable solutions. The upper and lower red branch corresponds to solutions $\tilde{\phi}=\pi,0$, respectively. The middle panel shows the critical bias currents $\gamma_{c,1}<0$ and $\gamma_{c,2}>0$ as a function of a for $L=1$. The bottom panel presents the critical eigenvalue of the nonuniform ground state as a function of γ for $a=0.495$ and $L=1$. Analytical approximations are also presented in dashed and dash-dotted lines.

The influence of the π facet length $2a$ on the existence diagram is indicated by the arrows, i.e., as a increases (decreases) toward $a_{c,\pi}$ the two lobes move according to the arrows (and vice versa). In the middle panel of Fig. 5, we plot the second critical bias current, $\gamma_{c,2}$, as a function of a.

Again, due to the cyclic symmetry, $\gamma_{c,2}$ can be obtained from $\gamma_{c,1}$ by rotating the curve by π radians, with the center of rotation at $(a,\gamma_{c,1})=(L/2,0)$.

In the infinite junctions discussed in Refs. 15, 17, and 19–21, it is shown that there are two critical currents, one critical value, which is related to a rearrangement of semifluxons due to the bias current pushing vortices toward each other, and another value, which corresponds to vortex breaking due to the bias current stretching vortices apart. Here, our $\gamma_{c,1}$ and $\gamma_{c,2}$ can correspond to either one, depending on the magnitude of $\gamma_{c,1}$ and $\gamma_{c,2}$. If $|\gamma_{c,n}|>|\gamma_{c,3-n}|$, $n=1,2$, then $\gamma_{c,n}$ and $\gamma_{c,3-n}$ will correspond to vortex breaking and vortex rearrangement, respectively.

In the bottom panel of Fig. 5, we plot the critical eigenvalue of the nonuniform ground state as a function of γ for $a=0.495$ and $L=1$. Interestingly, we observe that the lowest eigenvalue is attained at a nonzero bias current. This indicates that a nonuniform ground state can be made to be "more stable" by applying a bias current. Only if $a=L/2$ would a pair of semifluxons with $\gamma=0$ be most stable. On the same figure, we also plot our approximations (29), which qualitatively agree with the numerical results.

Studying further the saddle-node bifurcation between the nonuniform ground state and $\tilde{\phi}=\pi$ in Fig. 5, we observe that it is not the typical collision that leads to the definition of $\gamma_{c,2}$ for any L. When L is relatively large, we find that the upper branch does not necessarily correspond to a uniform solution. In Fig. 6, we consider another case for $L=10$ and $a=3$.

Starting on the middle branch from $\gamma=0$ and $\tilde{\phi}(0)\approx 3$, we then increase the bias current. At the critical bias current $\gamma_{c,2}$, i.e., $\gamma\approx 0.6$, we have a saddle-node bifurcation. Using our path following code, we follow the branch beyond the bifurcation point, from which we obtain that the branch does not correspond to a uniform solution. In the middle panel of Fig. 6, we plot the corresponding solutions for some values of γ. Considering the profile $\phi(x)$ at $\gamma=0$, we could conclude that it corresponds to a pair of semifluxons each bound to a fluxon. The profile is similar to the so-called semifluxon type 3, defined in Ref. 17 for an infinitely long 0-π Josephson junction. From our numerical computations (not shown here), the two branches seem to be distinguished by the ability of the junction of length $2L$ to support an additional fluxon on each side. The first critical value $\gamma_{c,1}$ corresponds to the collision between the nonuniform ground state and $\phi=0$. The bottom panel presents $\gamma_{c,1}$ and $\gamma_{c,2}$ as a function of a for $L=10$. An approximate expression for the critical currents is presented in dashed lines given by[15,30]

$$\gamma_{c,1} = -\sqrt{\frac{128}{27(\pi+2)}}(a-a_{c,0})^{3/2},$$

$$\gamma_{c,2} = \sqrt{\frac{128}{27(\pi+2)}}(a_{c,\pi}-a)^{3/2}, \tag{31}$$

where $a_{c,0}\approx\pi/4$ and $a_{c,\pi}\approx(L-\pi/4)$.

One may ask about using finite 0-π-0 Josephson junctions to observe macroscopic quantum tunneling and to build qubits. To answer the question, the reader is addressed to Refs.

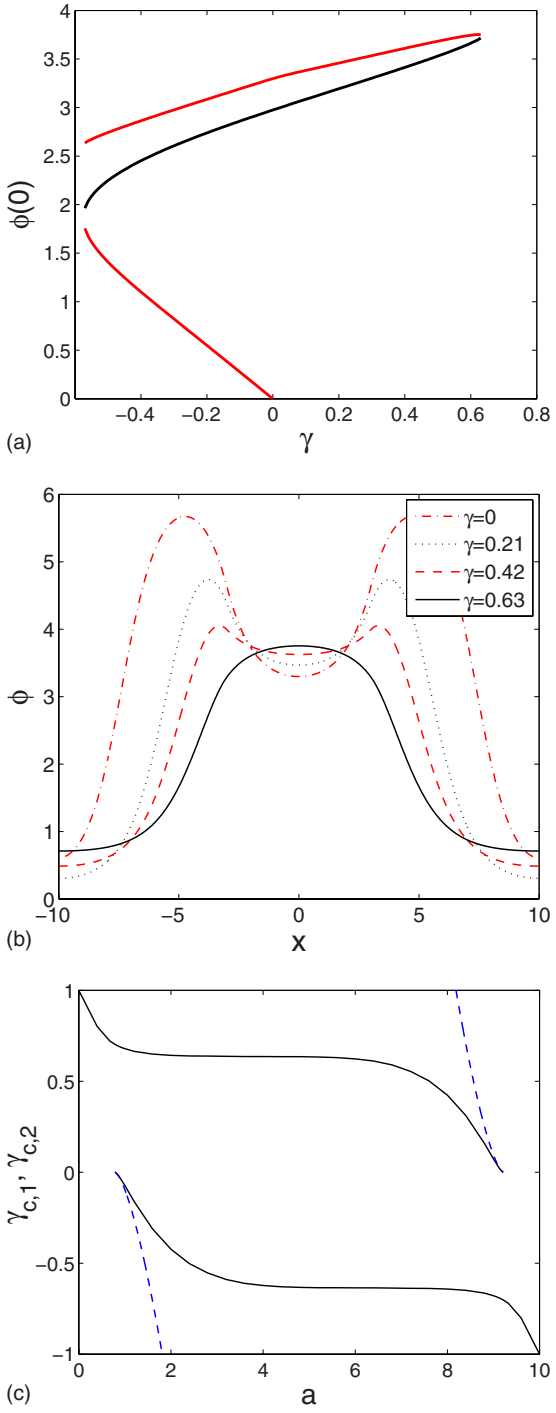

FIG. 6. (Color online) Top panel is the same as the top panel of Fig. 5, but for $L=10$ and $a=3$. Middle panel shows some of the corresponding solutions of the top branch for different values of γ. Bottom panel shows $\gamma_{c,1}<0$ and $\gamma_{c,2}>0$ as a function of a. Solid and dashed lines are numerical calculations and analytical approximations (31), respectively.

18 and 31, which consider quantum tunneling of a semifluxon in an infinite 0-π-0 junction and finite 0-π junction, respectively. It was concluded that both setups provide a good playground to observe macroscopic quantum tunneling. As for building a qubit, it will depend on the ratio between a and L. If $a\sim L$, the system considered here is not a promising

one, because it requires the junction length to be very small and in that small length region the flux is too tiny to be detected by current technology.[31] If $L \gg a$ and a is small enough, finite 0-π-0 junctions can be a good system for qubits.[18] It is then of interest to characterize the minimum value of L at which a finite 0-π-0 junction switches from being a good to a bad qubit system.

VI. CONCLUSION

We have investigated analytically and numerically 0-π-0 Josephson junctions on a finite domain. We have shown that there is an instability region for uniform solutions in which semifluxons are spontaneously generated. Using an Euler-Lagrange approximation, it has been shown that the existence of static semifluxons depends on the length of the junction, the facet length, and the applied bias current. In addition the critical eigenvalue of the semifluxons has been discussed. Numerical simulations have been presented, accompanying our analytical results.

In future investigations, the two dimensional version of Josephson junctions with phase-shifts, $\theta=\pi$ in some areas and $\theta=0$ elsewhere, will be considered. It is also of interest to apply results presented herein to 0-κ-0 junctions and compare them with the readily available experimental data.[19] These are works in progress and will be reported in future publications.

ACKNOWLEDGMENTS

We are grateful to Edward Goldobin and anonymous referees for their comments and suggestions that helped improve the manuscript. S.A. thanks the University of Malakand, Pakistan, for financial support.

APPENDIX: COEFFICIENT MATRICES

The coefficient matrices M_n, $n=1,2,3,4$, used to derive the 'continuous' and the discrete spectrum of $\phi=0,\pi$ are given by

$$M_1 = \begin{bmatrix} \cos[\hat{\alpha}(L-a)] & -\cos(\hat{\beta}a) & \sin(\hat{\beta}a) & 0 \\ \hat{\alpha}\sin[\hat{\alpha}(L-a)] & -\hat{\beta}\sin(\hat{\beta}a) & -\hat{\beta}\cos(\hat{\beta}a) & 0 \\ 0 & \cos(\hat{\beta}a) & \sin(\hat{\beta}a) & -\cos[\hat{\alpha}(a-L)] \\ 0 & -\hat{\beta}\sin(\hat{\beta}a) & \hat{\beta}\cos(\hat{\beta}a) & \hat{\alpha}\sin[\hat{\alpha}(a-L)] \end{bmatrix}, \tag{A1}$$

$$M_2 = \begin{bmatrix} \cosh[\hat{\gamma}(L-a)] & -\cos(\hat{\beta}a) & \sin(\hat{\beta}a) & 0 \\ \hat{\gamma}\sinh\hat{\gamma}(L-a) & -\hat{\beta}\sin(\hat{\beta}a) & -\hat{\beta}\cos(\hat{\beta}a) & 0 \\ 0 & \cos(\hat{\beta}a) & \sin(\hat{\beta}a) & \cosh[\hat{\gamma}(a-L)] \\ 0 & -\hat{\beta}\sin(\hat{\beta}a) & \hat{\beta}\sin(\hat{\beta}a) & \hat{\gamma}\sinh[\hat{\gamma}(a-L)] \end{bmatrix}, \tag{A2}$$

$$M_3 = \begin{bmatrix} \cos[\hat{\beta}(L-a)] & -\cos(\hat{\alpha}a) & \sin(\hat{\alpha}a) & 0 \\ \hat{\beta}\sin[\hat{\beta}(L-a)] & -\hat{\alpha}\sin(\hat{\alpha}a) & -\hat{\alpha}\cos(\hat{\alpha}a) & 0 \\ 0 & \cos(\hat{\alpha}a) & \sin(\hat{\alpha}a) & -\cos[\hat{\beta}(a-L)] \\ 0 & -\hat{\alpha}\sin(\hat{\alpha}a) & \hat{\beta}\sin(\hat{\beta}a) & -\hat{\beta}\sin[\hat{\beta}(a-L)] \end{bmatrix}, \tag{A3}$$

$$M_4 = \begin{bmatrix} \cos[\hat{\beta}(L-a)] & -\cosh\hat{\gamma}a & \sinh(\hat{\gamma}a) & 0 \\ \hat{\beta}\sin[\hat{\beta}(L-a)] & \hat{\gamma}\sinh(\hat{\gamma}a) & -\hat{\gamma}\cosh(\hat{\gamma}a) & 0 \\ 0 & \cosh(\hat{\gamma}a) & \sinh(\hat{\gamma}a) & -\cos[\hat{\beta}(a-L)] \\ 0 & \hat{\gamma}\sinh(\hat{\gamma}a) & \hat{\gamma}\cosh(\hat{\gamma}a) & \hat{\beta}\sin\hat{\beta}(a-L) \end{bmatrix}. \tag{A4}$$

*On leave from Department of Mathematics, University of Malakand, Chakdara, N.W.F.P., Pakistan.

[1] L. N. Bulaevskii, V. V. Kuzii, and A. A. Sobyanin, Pis'ma Zh. Eksp. Teor. Fiz. **25**, 314 (1977) [JETP Lett. **25**, 290 (1977)].

[2] L. N. Bulaevskii, V. V. Kuzii, and A. A. Sobyanin, Solid State Commun. **25**, 1053 (1978).

[3] O. Vávra, S. Gaži, D. S. Golubović, I. Vávra, J. Dérer, J. Verbeeck, G. Van Tendeloo, and V. V. Moshchalkov, Phys. Rev. B **74**, 020502(R) (2006).

[4] C. C. Tsuei and J. R. Kirtley, Rev. Mod. Phys. **72**, 969 (2000).

[5] A. Gumann, C. Iniotakis, and N. Schopohl, Appl. Phys. Lett. **91**, 192502 (2007).

[6] V. V. Ryazanov, V. A. Oboznov, A. Yu. Rusanov, A. V. Veretennikov, A. A. Golubov, and J. Aarts, Phys. Rev. Lett. **86**, 2427 (2001).

[7] M. Weides, M. Kemmler, H. Kohlstedt, R. Waser, D. Koelle, R. Kleiner, and E. Goldobin, Phys. Rev. Lett. **97**, 247001 (2006).

[8] M. Weides, M. Kemmler, E. Goldobin, D. Koelle, R. Kleiner, and H. Kohlstedt, Appl. Phys. Lett. **89**, 122511 (2006).

[9] J. J. A. Baselmans, A. F. Morpurgo, B. J. van Wees, and T. M. Klapwijk, Nature (London) **397**, 43 (1999).

[10] E. Goldobin, A. Sterck, T. Gaber, D. Koelle, and R. Kleiner, Phys. Rev. Lett. **92**, 057005 (2004).

[11] C. M. Pegrum, Science **312**, 1483 (2006).

[12] T. Ortlepp, Ariando, O. Mielke, C. J. M. Verwijs, K. F. K. Foo, H. Rogalla, F. H. Uhlmann, and H. Hilgenkamp, Science **312**, 1495 (2006).

[13] H. Hilgenkamp, Ariando, H. J. H. Smilde, D. H. A. Blank, G. Rijnders, H. Rogalla, J. R. Kirtley, and C. C. Tsuei, Nature (London) **422**, 50 (2003).

[14] S. M. Frolov, M. J. A. Stoutimore, T. A. Crane, D. J. Van Harlingen, V. A. Oboznov, V. V. Ryazanov, A. Ruosi, C. Granata, and M. Russo, Nat. Phys. **4**, 32 (2008).

[15] T. Kato and M. Imada, J. Phys. Soc. Jpn. **66**, 1445 (1997).

[16] A. Zenchuk and E. Goldobin, Phys. Rev. B **69**, 024515 (2004).

[17] H. Susanto, S. A. van Gils, T. P. P. Visser, Ariando, H. J. H. Smilde, and H. Hilgenkamp, Phys. Rev. B **68**, 104501 (2003).

[18] E. Goldobin, K. Vogel, O. Crasser, R. Walser, W. P. Schleich, D. Koelle, and R. Kleiner, Phys. Rev. B **72**, 054527 (2005).

[19] A. Dewes, T. Gaber, D. Koelle, R. Kleiner, and E. Goldobin, Phys. Rev. Lett. **101**, 247001 (2008).

[20] J. A. Boschker, M.S. thesis, University of Twente, 2006.

[21] A. B. Kuklov, V. S. Boyko, and J. Malinsky, Phys. Rev. B **51**, 11965 (1995); **55**, 11878 (1997).

[22] E. Goldobin, D. Koelle, and R. Kleiner, Phys. Rev. B **70**, 174519 (2004).

[23] E. Goldobin, H. Susanto, D. Koelle, R. Kleiner, and S. A. van Gils, Phys. Rev. B **71**, 104518 (2005).

[24] A. Buzdin and A. E. Koshelev, Phys. Rev. B **67**, 220504(R) (2003).

[25] H. Susanto, E. Goldobin, D. Koelle, R. Kleiner, and S. A. van Gils, Phys. Rev. B **71**, 174510 (2005).

[26] K. Buckenmaier, T. Gaber, M. Siegel, D. Koelle, R. Kleiner, and E. Goldobin, Phys. Rev. Lett. **98**, 117006 (2007).

[27] T. Gaber, K. Buckenmaier, D. Koelle, R. Kleiner, and E. Goldobin, Appl. Phys. A: Mater. Sci. Process. **89**, 587 (2007).

[28] J. Pfeiffer, T. Gaber, D. Koelle, R. Kleiner, E. Goldobin, M. Weides, H. Kohlstedt, J. Lisenfeld, A. K. Feofanov, and A. V. Ustinov, arXiv:0903.1046 (unpublished).

[29] R. W. D. Nickalls, Math. Gaz. **77**, 354 (1993).

[30] There is a typo in the expression of the critical current in Ref. 15.

[31] E. Goldobin, K. Vogel, W. P. Schleich, D. Koelle, and R. Kleiner, arXiv:0812.2394 (unpublished).